PIP2 mediates functional coupling and pharmacology of neuronal KCNQ channels

Robin Y. Kim[a], Stephan A. Pless[b], and Harley T. Kurata[a,1]

[a]Department of Pharmacology, Alberta Diabetes Institute, University of Alberta, Edmonton, AB, Canada T6G 2R3; and [b]Center for Biopharmaceuticals, Department of Drug Design and Pharmacology, University of Copenhagen, DK-2100 Copenhagen, Denmark

Edited by Ramon Latorre, Centro Interdisciplinario de Neurociencias de Valparaíso, Facultad de Ciencias, Universidad de Valparaíso, Valparaíso, Chile, and approved October 3, 2017 (received for review April 7, 2017)

Retigabine (RTG) is a first-in-class antiepileptic drug that suppresses neuronal excitability through the activation of voltage-gated KCNQ2–5 potassium channels. Retigabine binds to the pore-forming domain, causing a hyperpolarizing shift in the voltage dependence of channel activation. To elucidate how the retigabine binding site is coupled to changes in voltage sensing, we used voltage-clamp fluorometry to track conformational changes of the KCNQ3 voltage-sensing domains (VSDs) in response to voltage, retigabine, and PIP2. Steady-state ionic conductance and voltage sensor fluorescence closely overlap under basal PIP2 conditions. Retigabine stabilizes the conducting conformation of the pore and the activated voltage sensor conformation, leading to dramatic deceleration of current and fluorescence deactivation, but these effects are attenuated upon disruption of channel:PIP2 interactions. These findings reveal an important role for PIP2 in coupling retigabine binding to altered VSD function. We identify a polybasic motif in the proximal C terminus of retigabine-sensitive KCNQ channels that contributes to VSD–pore coupling via PIP2, and thereby influences the unique gating effects of retigabine.

electrophysiology | voltage-clamp fluorometry | KCNQ channel | potassium channel | epilepsy

KCNQ channels are voltage-gated potassium channels that play critical roles in regulating the excitability of neuronal, cardiac, and peripheral smooth muscle tissue. In the nervous system, KCNQ2 and KCNQ3 subunits are the primary constituents of M channels, which couple various receptor-mediated signaling pathways to neuronal excitability, usually via altered levels of membrane PIP2 (1, 2). Mutations in the KCNQ2 and KCNQ3 genes have been linked to forms of neonatal epilepsy of varying severity, from benign familial neonatal convulsions (BFNCs) to epileptic encephalopathy (3, 4). These channels are located at the axon initial segment and nodes of Ranvier, with biophysical hallmarks, including activation at subthreshold potentials, lack of inactivation, and relatively slow gating kinetics (5, 6). Recently, retigabine (RTG) has emerged as a relatively safe and effective antiepileptic drug, demonstrating the therapeutic potential for activating neuronal KCNQ channels to attenuate excitability in disorders such as epilepsy (7–9).

Retigabine and its close structural analog flupirtine are the first voltage-gated K^+ channel openers approved for use in humans. A detailed understanding of the mechanism of action of these drugs may guide the development of more effective and specific channel activators. Previous studies have demonstrated that retigabine stabilizes the open state of KCNQ2–5 channels, reflected in a marked shift of the voltage dependence of channel activation to more negative potentials and in some cases, an increase of maximal open probability (10–13). The retigabine binding site has been characterized in several reports, highlighting the importance of a binding pocket within the pore domain anchored by a critical hydrogen bond interaction between the drug and an S5 tryptophan residue that is conserved in retigabine-sensitive KCNQ channels (KCNQ2–5) (14–17).

KCNQ channel:PIP2 interactions are essential for channel activity and have also been highlighted as important modulators of pharmacological sensitivity to certain KCNQ activators (18). Retigabine effects on KCNQ channels rely on the presence of sufficient PIP2, while certain other activators such as Zn-pyrithione appear to rescue KCNQ currents in the nominal absence of PIP2 (18). The molecular mechanisms that govern functional interactions between KCNQ activators, the KCNQ channel voltage-sensing apparatus, and the essential phospholipid PIP2 have not been investigated.

To investigate the mechanisms underlying the dramatic effects of retigabine on the voltage sensitivity of KCNQ channels, we employed voltage-clamp fluorometry (VCF) to directly measure conformational changes of the voltage-sensing domain (VSD) and relate these changes to function of the pore in KCNQ3 channels. By assessing the impact of voltage, retigabine, PIP2 levels, and mutation of potential cytosolic residues involved in VSD–pore coupling, we provide mechanistic insights into the functional and pharmacological properties of KCNQ channels.

Results

Voltage-Clamp Fluorometry of KCNQ3 Channels. The VCF approach requires introduction of a fluorophore in a region that is sensitive to voltage-dependent conformational changes (Fig. 1*B*, *Bottom*). To generate a useful KCNQ3* (refers to KCNQ3[Ala315Thr]) [see *Methods* (19)] construct for VCF, we tested a series of cysteine mutants throughout the extracellular S3–S4 linker (Fig. 1*A*). This region was highly sensitive to mutation, with several mutants

Significance

Despite the availability of many drugs to treat epilepsy, nearly one-third of patients are not responsive to pharmacotherapy. Retigabine (RTG) is the first approved antiepileptic drug that acts by promoting activation of potassium channels, specifically targeting neuronal KCNQ channels that are regulated by both voltage and the membrane phospholipid PIP2. A deeper understanding of the mechanism of action of RTG will enable future development of this unique drug class. In this study, we combine electrophysiology recordings with fluorometric measurements of KCNQ channel conformation to reveal channel features that contribute to the dramatic effects of RTG. Our findings demonstrate that a PIP2-dependent interaction between the pore-forming and voltage-sensing components of the channel is required for optimal RTG action.

Author contributions: R.Y.K., S.A.P., and H.T.K. designed research; R.Y.K. and H.T.K. performed research; R.Y.K., S.A.P., and H.T.K. analyzed data; and R.Y.K., S.A.P., and H.T.K. wrote the paper.

The authors declare no conflict of interest.

This article is a PNAS Direct Submission.

[1]To whom correspondence should be addressed. Email: kurata@ualberta.ca.

This article contains supporting information online at www.pnas.org/lookup/suppl/doi:10.1073/pnas.1705802114/-/DCSupplemental.

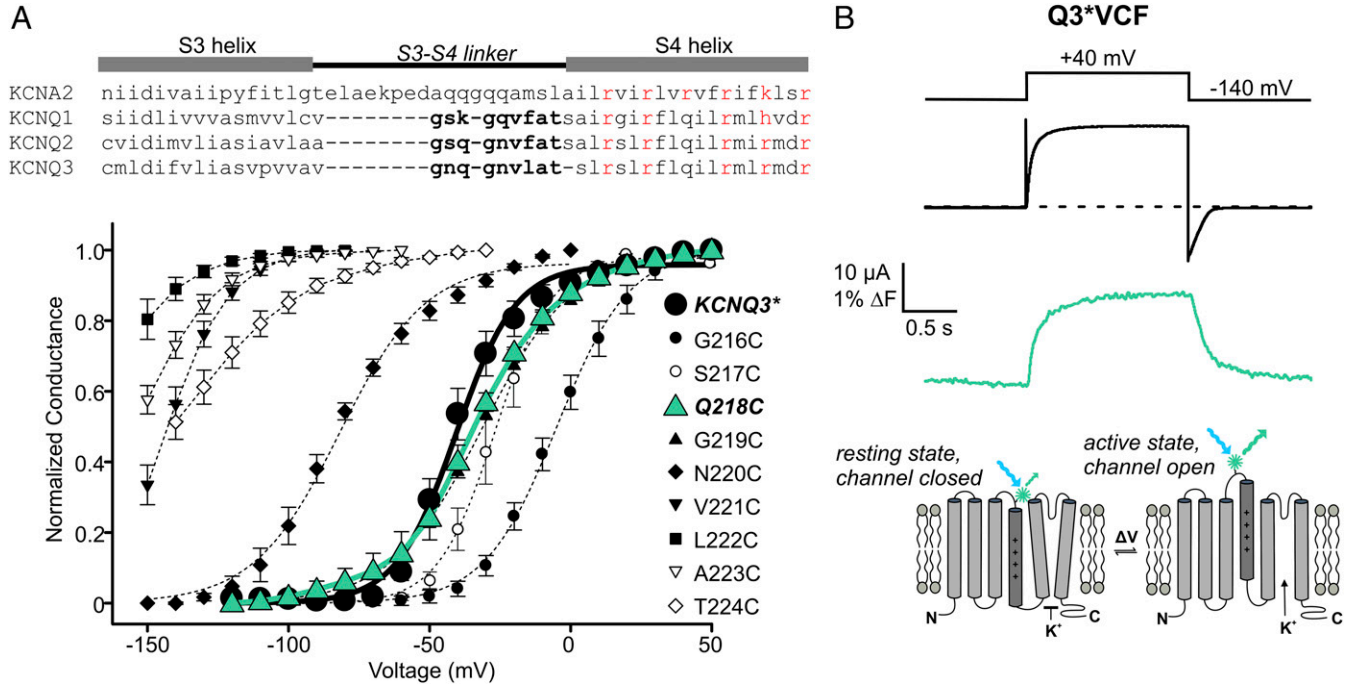

Fig. 1. Cysteine scan mutagenesis of KCNQ3* S3–S4 linker residues and identification of Q218C as the ideal position for fluorophore labeling. (*A*) Conductance–voltage relationships were determined for a series of cysteine mutants in the S3–S4 linker of KCNQ3* ($n = 3$–4 for each mutant, error bars represent SEM). (*B*, *Top*) Exemplar traces of ionic current (black) and fluorescence (green) from a *X. laevis* oocyte expressing KCNQ3*[218C] (abbreviated as Q3*VCF in text and all figures), labeled with Alexa-488 maleimide and depolarized to +40 mV. (*Bottom*) Cartoon illustration of the VCF technique.

generating ~100-mV hyperpolarizing gating shifts (Fig. 1*A*), although we have not explored these large effects any further. The KCNQ3*[G219C] and [Q218C] mutations were nearly indistinguishable from KCNQ3* channels in terms of their voltage dependence (Fig. 1*A*) and retigabine response. G219C is homologous to the mutation successfully used in several VCF studies of KCNQ1 (20–22). Both the Q218C and G219C sites reported fluorescence changes, but the most robust signals were obtained from channels with Q218C (labeled with Alexa Fluor-488 maleimide, Fig. 1*B*). This construct was used throughout the study and is abbreviated as Q3*VCF. We have also tested analogous mutations in KCNQ2 and KCNQ2/KCNQ3 heteromeric channels, but the expression of these channels is significantly lower than KCNQ3* and we have not successfully generated VCF recordings from these other KCNQ subtypes.

Overlapping Voltage Dependence of the KCNQ3 Voltage Sensor and Pore. Fluorescence-voltage relationships of Q3*VCF were generated by holding oocytes at a depolarized potential (+20 mV) and stepping to a range of hyperpolarizing potentials. This was required because the strongly shifted voltage dependence of activation of KCNQ3* in retigabine required long interpulse intervals at very negative voltages to achieve a stable fluorescence baseline, leading to technical difficulties with recording. We observed a direct overlap in the voltage dependence of the fluorescence change and conductance (Fig. 2*A*). This close overlap of conductance and fluorescence persists in saturating retigabine concentrations, as both are shifted equally by approximately −60 mV (Fig. 2 *A* and *E*, note that the absolute $V_{1/2}$ reported here differs somewhat from typical experiments because of the altered voltage step protocol that was needed). To highlight this gating shift, sweeps to −60 mV are depicted in red (Fig. 2*A*), where retigabine immobilization of VSD movement is evident. Retigabine decelerates channel closure and voltage sensor deactivation (Fig. 2*B*) and modestly accelerates activation of current and voltage sensor fluorescence (Fig. 2*C*). Similar to KCNQ1 (without KCNE1), but unlike the canonical model Kv channel *Shaker*, there is a fairly close correlation of voltage sensor and current signals (ionic currents are overlaid as dashed lines), although the voltage sensor fluorescence typically exhibits a minor slow kinetic component (Fig. 2 *B* and *C*) and mild sigmoidal VSD deactivation kinetics in retigabine that are not apparent in ionic currents (Fig. 2*B*). Unexpectedly, we also observed that retigabine increases the magnitude of the fluorescence signal (ΔF) in response to a given depolarization (Fig. 2*F*). As an important control, all effects of retigabine on fluorescence and currents are abolished when retigabine binding is disrupted by the W265F mutation (Fig. 2 *D*–*F*), demonstrating the requirement for retigabine binding to the pore.

PIP2 Influences Pore Coupling and VSD Movement. The membrane phospholipid PIP2 is an essential cofactor and regulator of KCNQ channels. PIP2 is required for pore opening, and its hydrolysis underlies G_q-coupled receptor-mediated channel inhibition (23, 24). Recent investigations of KCNQ1 suggest this requirement reflects PIP2-dependent conformational coupling of the VSD and pore (22, 25). Therefore, we reasoned that PIP2-dependent coupling might influence transduction of retigabine binding from the pore to the voltage sensor. To test the influence of PIP2, we coexpressed Q3*VCF with the *Ciona intestinalis* voltage-sensitive phosphatase CiVSP, allowing time-resolved control of PIP2 levels using depolarization to activate the phosphatase (26). At depolarized potentials that activate CiVSP, we observed a fluorescence deflection that persists even after pore closure is induced by PIP2 depletion (Fig. 3*A*). A subsequent identical depolarization produces a similar fluorescence change but little current, illustrating that PIP2 is not required for voltage sensor movement (Fig. 3*A*).

There are important quantitative differences in voltage sensor fluorescence signals after PIP2 reduction. There is a pronounced increase in the magnitude of the fluorescence signal that occurs simultaneously with PIP2 reduction (Fig. 3*B*). This is not immediately obvious in Fig. 3*A* because the CiVSP-mediated

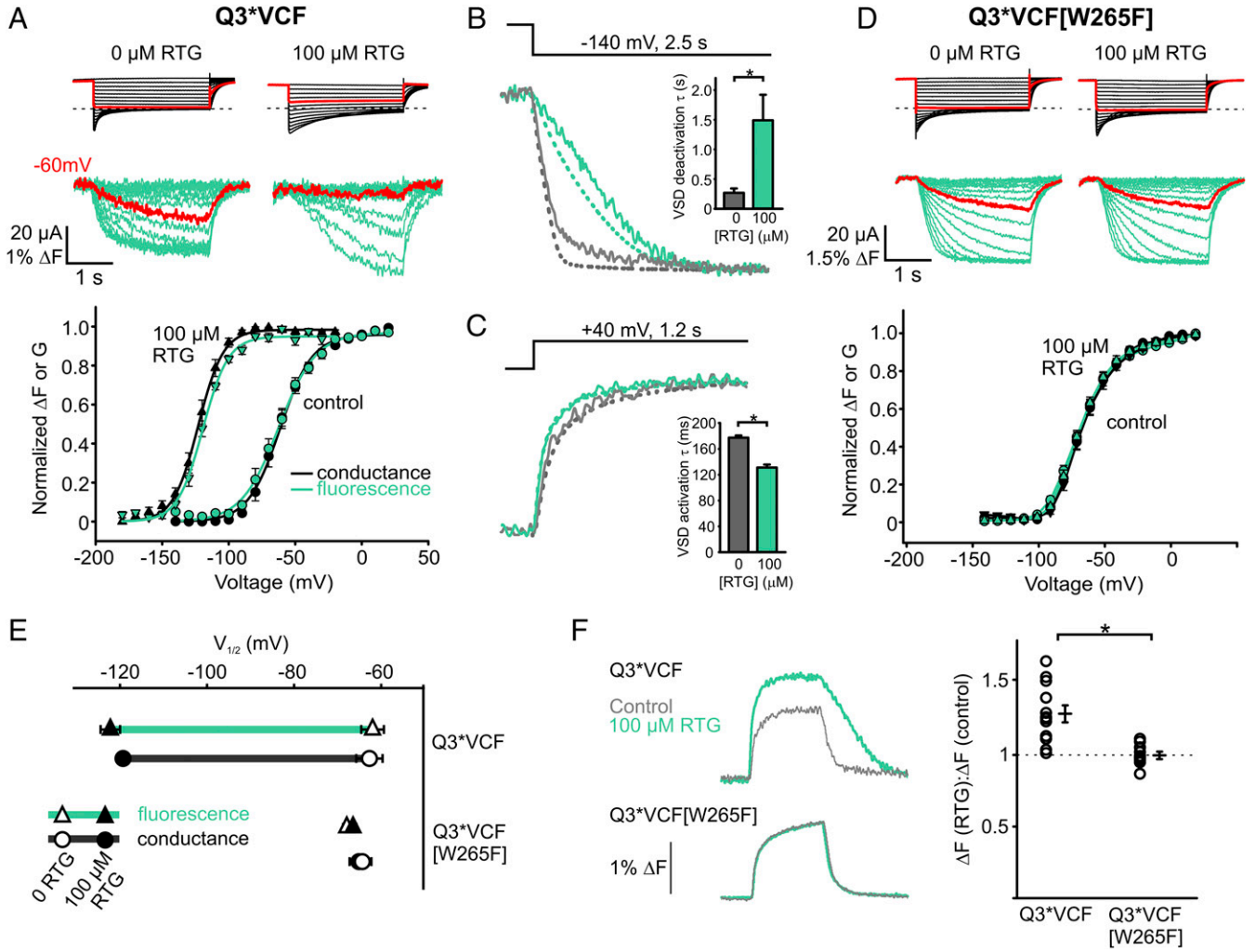

Fig. 2. Characterization of retigabine (RTG) effects on Q3*VCF fluorescence. (*A*) Oocytes were clamped at a holding potential of +20 mV [control (ctrl) condition] or −20 mV (100 μM RTG) and hyperpolarized in −10 mV steps to for 3 s. Exemplar current (black) and fluorescence (green) traces (*Top*) and normalized ΔF or G (tail currents) are displayed (*Bottom*) ($n = 6$ or 5, ctrl/RTG). (*B* and *C*) Sample fluorescence sweeps (solid lines) and currents (dashed lines) and summary of deactivation kinetics at −140 mV (τ: −254 ± 24 ms in control and 1,440 ± 180 ms in RTG, $n = 9$ each) and activation kinetics at +40 mV (τ: 178 ± 4 ms in control and 130 ± 5 ms in RTG, $n = 5$ each) in control (gray) or 100 μM RTG (green). (*D*) RTG effects on Q3*VCF [W265F] ($n = 7$ or 8, ctrl/RTG) using the same protocols as in *A*. (*E*) Summary of $V_{1/2}$ values (ΔF and G) for Q3*VCF and Q3*VCF[W265F] ± 100 μM RTG (Q3*VCF: −62.0 ± 3 mV and −63 ± 3 mV for ΔF and G in control, respectively, −122 ± 3 mV and −119 ± 2 mV for ΔF and G in 100 μM RTG; Q3*VCF[W265F]: −65 ± 2 mV and −68 ± 2 mV for ΔF and G in control, −64 ± 2.1 mV and −67 ± 2 mV for ΔF and G in 100 μM RTG). (*F*) Fluorescence sweeps and ΔF(RTG)/ΔF(control) summary data from depolarizations to +40 mV from −140 mV in control (gray) or 100 μM RTG (green) for Q3*VCF (1.28 ± 0.06, $n = 12$) and Q3*VCF[W265F] (1.00 ± 0.02, $n = 11$).

PIP2 depletion is occurring on approximately the same time scale as activation of current and fluorescence. However, in oocytes with slower current rundown kinetics, there is a clear correlation between the time course of current decay and a second phase of fluorescence unquenching at +100 mV, where CiVSP becomes activated (Fig. 3*B* and Fig. S1). This effect is also apparent in nonuniformly voltage-clamped oocytes, where artifactual irregular kinetics of CiVSP-mediated current decay closely mirror kinetics of fluorescence unquenching (Fig. S1). To confirm that this unexpected behavior was due to PIP2 reduction, we performed the same protocol in the absence of CiVSP (Fig. 3*C*), and observed that depolarizations to +100 mV (compared with +20 mV) elicited fluorescence signals with a much smaller increase in magnitude and lacking the unquenching phase (Fig. 3 *B*–*D*). Lastly, we performed a triple pulse protocol of two depolarizations to +20 mV, separated by a depolarization to +100 mV (to reduce PIP2). In this experiment, PIP2 reduction consistently facilitates the fluorescence signal in the second +20-mV depolarization (Fig. 3*F*). A final important observation, revisited later, is that PIP2 depletion causes acceleration of voltage sensor deactivation at −100 mV (Fig. 3*G*), while activation kinetics are unaffected. Taken together, these results highlight that PIP2 influences the dynamics and conformations sampled by the VSD and is required for voltage-dependent opening.

Retigabine Protects Channels from CiVSP-Mediated Rundown. We next examined how PIP2 influences transduction of retigabine binding to changes in voltage sensing. We began by using CiVSP coexpression to reduce PIP2 and observed that CiVSP effects are significantly weakened in the presence of retigabine (Fig. 4*A*). In this experiment, voltage steps between −140 mV and +100 mV were delivered, followed by a test pulse to −20 mV to observe the extent of PIP2 reduction after different prepulses. In control conditions, this yields a characteristic bell-shaped relationship (27), reflecting channel activation at modest depolarizations (insufficient to activate CiVSP), and strong current inhibition at

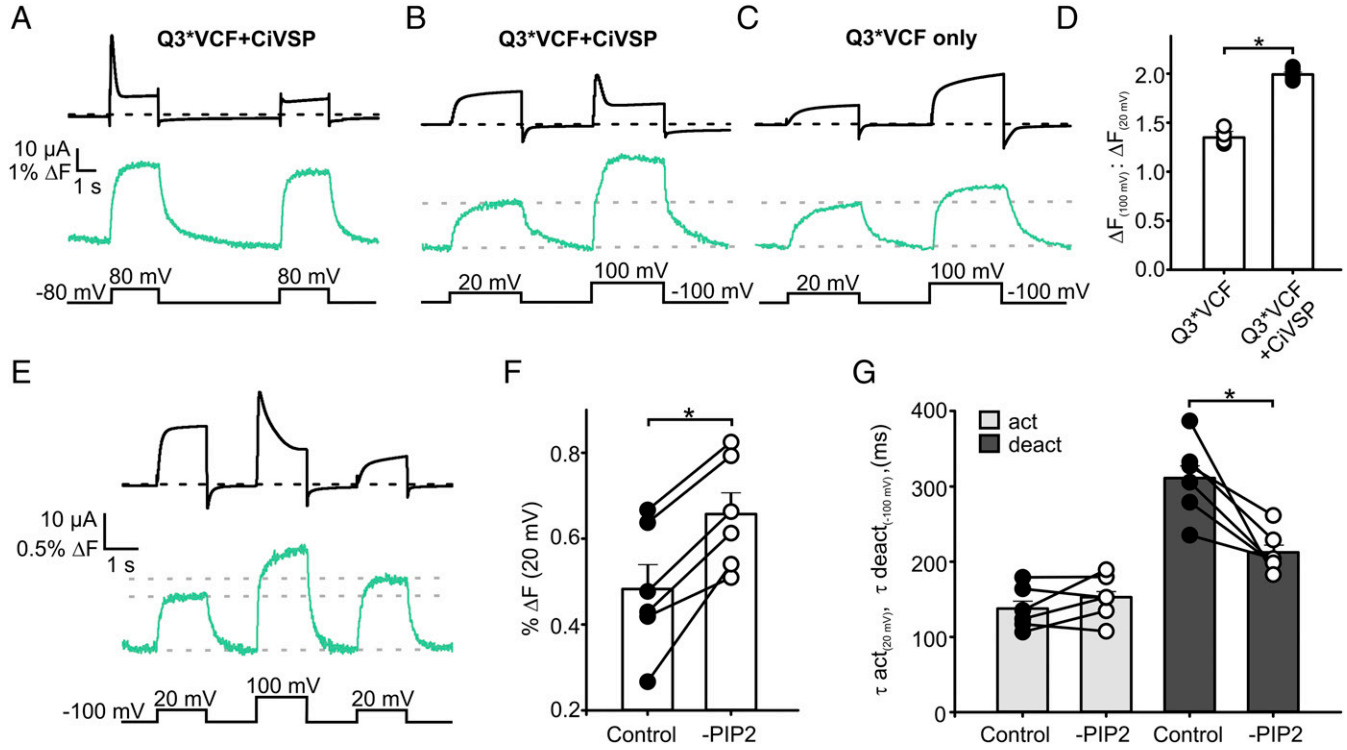

Fig. 3. PIP2 depletion alters Q3*VCF fluorescence. (*A*) Exemplar traces from an oocyte expressing Q3*VCF + CiVSP, subjected to consecutive depolarizations to +80 mV, highlighting the effects of PIP2 depletion on current (black) and fluorescence (green). (*B* and *C*) Exemplar current and fluorescence traces of Q3*VCF expressed alone (*C*) or with CiVSP (*B*), subjected to depolarizations causing weak (+20 mV) or strong (+100 mV) activation of CiVSP. PIP2 depletion at highly depolarized potentials produces a significant increase in ΔF. (*D*) Summary of ΔF (+100 mV)/ΔF (+20 mV) for Q3*VCF and Q3*VCF + CiVSP (1.35 ± 0.05 and 1.99 ± 0.02, respectively, $n = 4$ and 5). (*E*) A triple-pulse protocol was applied to assess the impact of PIP2 depletion on ΔF magnitude and kinetics, by comparing the fluorescence signal elicited by a +20 mV depolarization, before and after PIP2 depletion by a pulse to +100 mV. (*F*) Summary graph displaying the increase in ΔF magnitude at +20 mV after a PIP2 depleting +100 mV pulse, including paired data points from individual oocytes (0.48 ± 0.06% ΔF prerundown, 0.66 ± 0.05% ΔF postrundown). (*G*) Kinetics of activation (+20 mV) and deactivation (−100 mV) before and after a PIP2-depleting pulse (τ_{act}: 138 ± 12 ms in control, 153 ± 12 ms in reduced PIP2; τ_{deact}: 311 ± 21 ms in control, 212 ± 12 ms in reduced PIP2).

positive voltages where CiVSP activity is higher. In the presence of retigabine, channel activation is observed at more negative voltages, as expected (due to the retigabine-mediated shift in channel activation). More importantly, there is prominent "protection" against current rundown at positive voltages (Fig. 4*A*), reminiscent of previously reported protective effects of retigabine against M1 receptor-mediated current rundown (28). This effect is absent in the W265F mutant (Fig. 4*B*), demonstrating that retigabine does not directly inhibit CiVSP, but instead appears to protect channel-associated PIP2.

We exploited the retigabine protection effect to investigate reciprocal influences of PIP2, retigabine, and potential PIP2-interacting residues. The cytoplasmic side of KCNQ channels has a high density of basic residues potentially involved in PIP2 interaction, and we have focused on the S2–S3 linker and the proximal C terminus immediately following the S6 helix (Fig. 4 *F* and *G*). We performed a charge neutralization scan by mutating positively charged residues to alanine (Fig. 4 *C*–*E*). In addition, we modified a cluster of basic residues ("KRRK motif") in the proximal KCNQ3 C terminus, with sequential double alanine substitutions, along with a neutralization of all four residues (termed S6-AARK, S6-KRAA, S6-AAAA). Relative to KCNQ1, there is a slightly different arrangement of positively charged side chains in the S2–S3 linker sequence of KCNQ2–5, and more positive charges in the vicinity of the C-terminal KRRK cluster (Fig. 4 *F* and *G*).

We reasoned that mutation of residues important for PIP2-mediated coupling of the pore and VSD might also alter retigabine protection against CiVSP-mediated rundown. In the absence of retigabine, most mutants exhibited prominent CiVSP-mediated rundown (Fig. 4*C*). However, we observed a range of retigabine-mediated protection (Fig. 4*D*). Most significantly, multiple mutations in the proximal C terminus abolished retigabine-induced protection from CiVSP (Fig. 4 *C*–*E*). CiVSP-mediated rundown of the R364A, H367A, S6-AARK, and S6-KRAA mutants was insensitive to retigabine (Fig. 4*E*). Also, in control conditions, the onset of CiVSP-mediated rundown of these mutants (shown in blue in Fig. 4*C*) occurred at more negative voltages than retigabine-protected channels. Thus, disruption of basic C-terminal residues generally led to greater susceptibility to CiVSP in both control and retigabine conditions. An interesting exception in this region was the K358A mutant, which exhibited very little CiVSP-mediated rundown in either control or retigabine conditions (Fig. 4 *C*–*E*). The protection effect is retained to varying degrees for all S2–S3 mutants, with R190A exhibiting slightly weaker protection against CiVSP-mediated rundown (Fig. 4*E*). We also measured the effects of retigabine on the kinetics of CiVSP rundown in more detail (Fig. S3). The kinetics of the protection effect were noteworthy, as retigabine did not notably affect the rate of CiVSP-mediated rundown in any of the mutants. Rather, retigabine application led to a sustained plateau current in retigabine-protected channels (such as the S2–S3 linker mutants), in contrast to the complete current rundown observed in many C-terminal mutants (Fig. S3).

Basic characterization of the charge neutralization mutants was consistent with the retigabine protection assay. Neutralization of S2–S3 linker charges had modest effects on current expression,

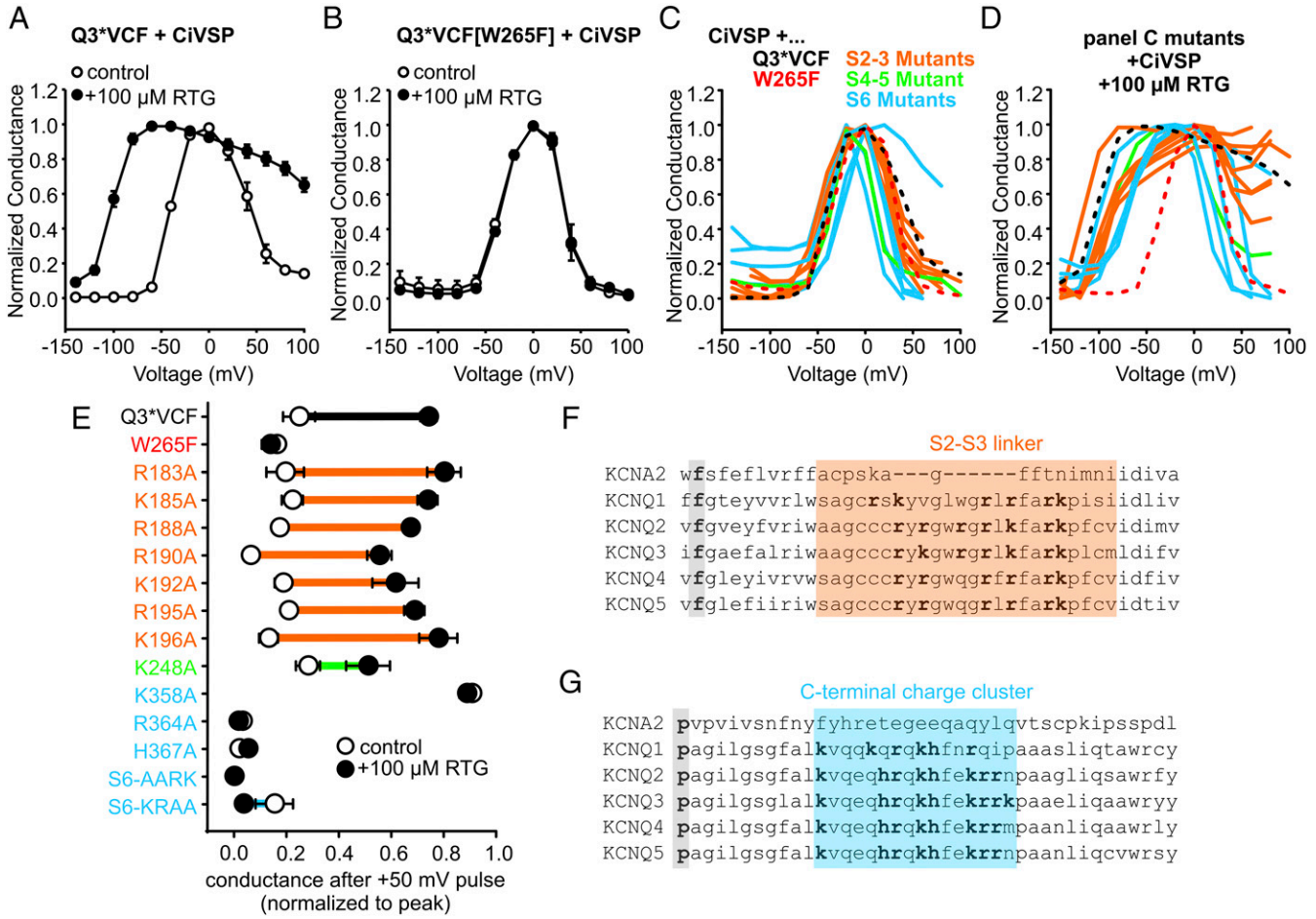

Fig. 4. RTG-induced strengthening of channel:PIP2 interactions relies on C-terminal basic residues. (*A* and *B*) Oocytes coexpressing CiVSP with Q3*VCF (*A*) or Q3*VCF[W265F] (*B*), were pulsed between −140 and +100 mV for 2 s, followed by a test pulse to −20 mV, in control or 100 μM RTG ($n = 5$ and $n = 6$, respectively). Test pulse currents were normalized to the voltage where maximal channel activity was observed. (*C* and *D*) Identical protocols as described in *A* and *B* were delivered to oocytes expressing CiVSP together with Q3*VCF mutants in the S2–S3 linker, S4–S5 linker, or C terminus as indicated (shown in *E* and color coded by region), in control (*C*) or 100 μM RTG (*D*, $n = 4$–6 for all constructs). (*E*) Summary of CiVSP induced current rundown at +50 mV, using a protocol described in Fig. S3. These findings highlight the necessity of C-terminal residues in enabling RTG-mediated PIP2 rundown protection. (*F* and *G*) Sequence alignments highlighting the high density of basic residues in the S2–S3 linker (*F*, the gating charge transfer center phenylalanine residue is highlighted in gray for orientation) and C termini (*G*, a conserved kinking proline is highlighted in gray for orientation) of Kv1.2 and KCNQ1–5 channels.

$V_{1/2}$ of activation, or response to 100 μM retigabine (Fig. S2). In contrast, mutation of K248 (S4–S5 linker) and the majority of basic residues in the proximal C terminus had profound effects: all except K358A led to >50% reduction in currents, with K248A, R364A, S6-AARK, and S6-AAAA causing >85% reduction in currents (Fig. S2*A*). The S6-AAAA mutation was the most disruptive, as currents were undetectable in the absence of retigabine, although 100 μM retigabine rescued a small amount of ionic current and enabled the collection of conductance–voltage relationships (Fig. S2*B*). With the exception of K358A, proximal C terminus mutants attenuated (but did not abolish) the retigabine-induced shift in $V_{1/2}$ of activation. We highlight that the C-terminal mutants that were disruptive to current are the same mutants that abolished retigabine-mediated protection against CiVSP (Fig. 4 *C*–*E*) and also exhibit CiVSP-mediated rundown at less depolarized voltages (Fig. 4 *C* and *D*). Taken together, these findings suggest an important relationship between PIP2 and transduction of retigabine effects to the voltage sensor.

The C Terminus Is Essential for Normal Pore–VSD Coupling. We investigated the role of the C terminus in the transduction of retigabine effects in more detail using VCF. Despite extremely small currents from KRRK cluster mutants, these channels generated robust voltage-dependent fluorescence signals that were consistently much larger than signals from Q3*VCF (Fig. 5*A*). These observations suggest that the mutants express very well at the cell surface but are likely hampered by weak VSD–pore coupling. We also observed marked retigabine enhancement of currents in these mutants (Fig. 5*C*), suggesting a large proportion of channels fail to open in control conditions, but can be partially rescued by retigabine.

There were several pronounced differences in the effects of retigabine on the C-terminal mutant channels. Firstly, the retigabine-mediated shift of the conductance–voltage relationship was weakened relative to Q3*VCF (Fig. 5 *B* and *D*), and this effect correlated with the impact of mutations on overall channel function (KRAA channels were more strongly shifted by retigabine than AARK or AAAA channels). The shift of the fluorescence–voltage relationship was also significantly disrupted in these mutants (e.g., $\Delta V_{1/2} = -57 \pm 3$ mV for Q3*VCF; -30 ± 4 mV for S6-AARK). Particularly in S6-AARK and S6-AAAA mutants, fluorescence was less disrupted than conductance, resulting in a ∼10-mV dissociation of FV and GV that became apparent in the presence of retigabine (Fig. 5 *B* and *D*). The FV

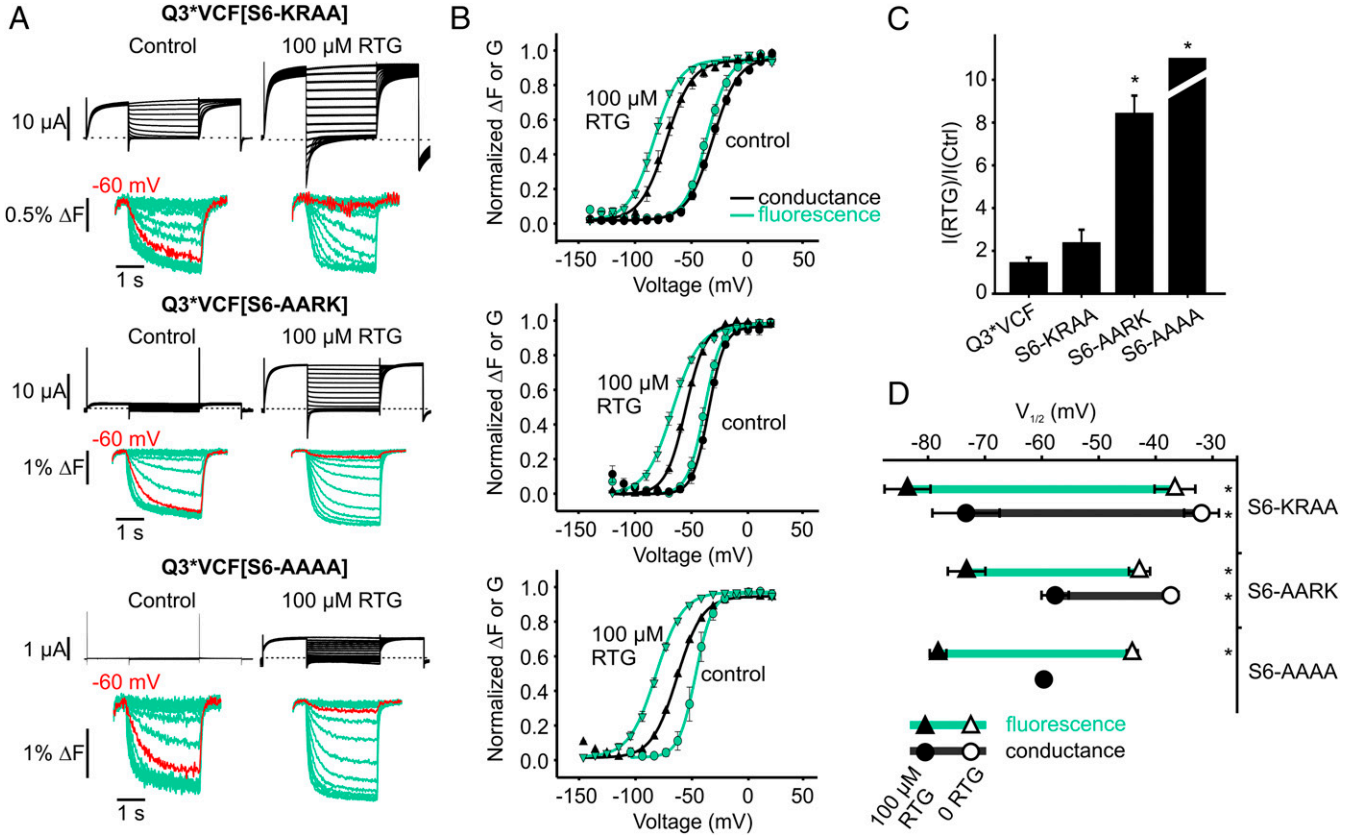

Fig. 5. RTG effects on the VSD are partially mediated by C-terminal residues involved in VSD–pore coupling. (*A*) Exemplar current (black) and fluorescence (green) recordings obtained from Q3*VCF with charge neutralizations in their S6-KRRK motifs. Voltage steps to −60 mV are highlighted red in all conditions to illustrate the RTG-induced shifts in the voltage dependence of ΔF, which persist even as pore function is progressively lost. (*B*) Summary graphs of the voltage and RTG dependence of ΔF and G for mutants shown in *A* (n = 4–10 per mutant). (*C*) Summary of 100 μM RTG-induced enhancement of current at +20 mV for S6-WT (1.4 ± 0.3), S6-KRAA (2.3 ± 0.6), S6-AARK (8.4 ± 0.9), and S6-AAAA (immeasurable due to absence of currents in 0 RTG) (n = 4–10). (*D*) $V_{1/2}$ values for ΔF and G, highlighting the RTG-mediated shift in fluorescence (green lines). $\Delta V_{1/2}$ for FV relationships were −57 ± 3 mV (Q3*VCF), −41 ± 7 mV (S6-KRAA), −30 ± 4 mV (S6-AARK), and −34 ± 2 mV (S6-AAAA). $\Delta V_{1/2}$ for GV relationships were −60 ± 4 mV (Q3*VCF), −47 ± 5 mV (S6-KRAA), and −20 ± 3 mV (S6-AARK) (*P < 0.05 for $\Delta V_{1/2}$ compared with Q3*VCF FV or GV as indicated, using ANOVA and Dunnett's post hoc test).

and GV relationships were also significantly steeper in the C-terminal mutants (in control conditions, Q3*VCF fluorescence–voltage relationship was fit with an effective valence of 1.95 ± 0.08 elementary charges vs. the S6-AARK valence of 3.8 ± 0.1). Using the effective valence and $V_{1/2}$ of Boltzmann fits to the fluorescence–voltage relationships, we estimated the energetic effects of retigabine on the VSD equilibrium for Q3*VCF (ΔΔG = −5.2 ± 0.3 kcal/mol), S6-AARK (ΔΔG = 0.2 ± 0.3 kcal/mol), and S6-AAAA (ΔΔG = 0.08 ± 0.17 kcal/mol), indicating a strongly attenuated voltage sensor effect of retigabine in these mutants.

KRRK cluster mutants markedly altered the effects of retigabine on VSD kinetics, shown by a detailed comparison of Q3*VCF and S6-AARK fluorescence (Fig. 6). In Q3*VCF channels, retigabine causes dramatic deceleration of fluorescence deactivation (Figs. 2*B* and 6 *A* and *B*), and leads to the appearance of mild sigmoidal deactivation kinetics (loss of exponential decay kinetics). In S6-AARK channels, retigabine-mediated effects on VSD deactivation are strongly attenuated (Fig. 6 *A* and *B*), as no pronounced deceleration or sigmoidal kinetics are observed in the fluorescence signal. In contrast, retigabine effects on voltage sensor activation kinetics are preserved (even somewhat accentuated) in S6-AARK mutants, relative to Q3*VCF (Fig. 6 *C* and *D*). Taken together these data suggest that retigabine has dichotomous effects on voltage sensor deactivation (possibly mediated by a C-terminal interaction with PIP2) and activation (likely mediated by a PIP2-independent mechanism).

Residual PIP2-Independent Coupling of Retigabine. Mutations in the KRRK cluster attenuate but do not completely uncouple effects of retigabine on the voltage sensor (Fig. 5 *B* and *D*). To rule out the possibility of a persistent PIP2-mediated coupling of retigabine effects (due to incomplete effects of the C-terminal mutations), we exploited the increased susceptibility of S6-AARK channels to CiVSP-mediated PIP2 rundown (Fig. 4). With CiVSP coexpression, we recorded Q3*VCF[S6-AARK] fluorescence using a holding potential of +80 mV (for sustained CiVSP activation), to test the voltage sensor effects of retigabine with maximal PIP2 reduction (Fig. 7). There were no detectable KCNQ3 currents, despite very pronounced fluorescence signals (Fig. 7*A*), indicating that CiVSP was functioning properly. These data demonstrate that even in the absence of PIP2, retigabine stabilizes VSD activation leading to a −31.1 ± 1.9 mV $\Delta V_{1/2}$ of the fluorescence–voltage relationship (Fig. 7*B*). This was similar to the shift observed in S6-AARK channels without CiVSP (Fig. 5*D*, $\Delta V_{1/2}$ = −30.4 ± 3.8 mV), but significantly less than the maximal shift of −57 ± 3 mV in Q3*VCF.

Structural Basis for PIP2-Mediated VSD–Pore Coupling. Overall, the charge neutralization scan highlights the importance of charged residues in the proximal C terminus for channel function and suggest this region is important for normal transduction of retigabine binding to altered VSD function (Figs. 4–6). The recent appearance of a cryo-EM structure of the related KCNQ1 channel

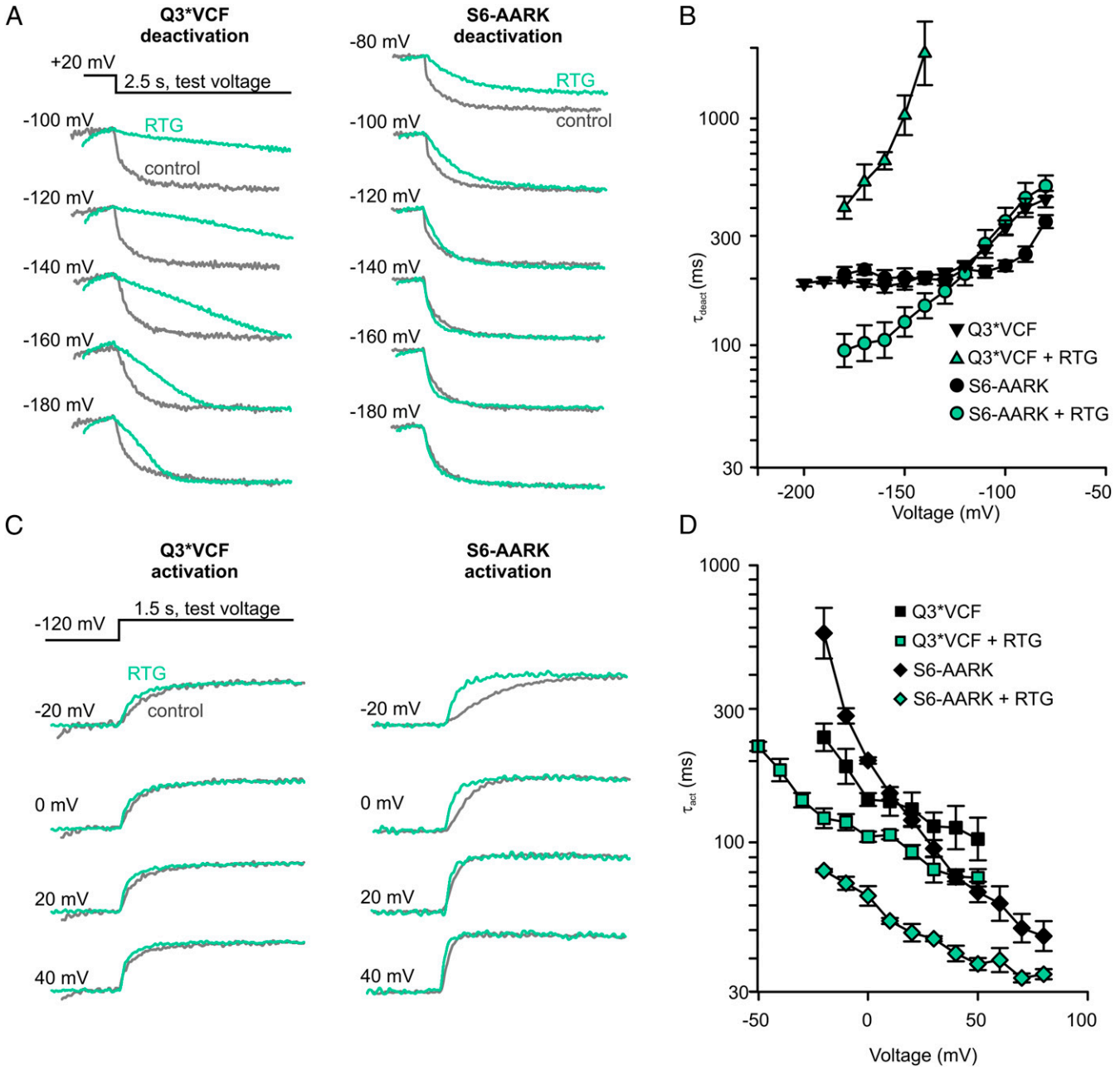

Fig. 6. Kinetic effects of retigabine in Q3*VCF and S6-AARK mutant channels. (*A*) Exemplar sweeps depicting VSD fluorescence deactivation kinetics at indicated voltages in Q3*VCF and S6-AARK channels, and the influence of retigabine. (*C*) Exemplar sweeps depicting VSD fluorescence activation kinetics at indicated voltages in Q3*VCF and S6-AARK channels. Summary data (mean + SEM) is presented in *B* and *D* (n = 5 per condition).

in complex with calmodulin provides a very useful template for understanding the orientation of the KCNQ channel C terminus relative to the pore and VSD (29) (Fig. 8). We originally suspected that the rich density of positively charged side chains in the S2–S3 linker might influence channel function and retigabine sensitivity via PIP2 interactions. However, our experimental findings suggest this is not a prominent effect (Fig. 4 and Fig. S2), and in the cryo-EM structure this motif appears to be primarily involved in forming an interface with calmodulin rather than interacting with the C terminus. The KRRK cluster is located just before an IQ-like motif previously suggested to mediate calmodulin interactions with KCNQ channels (30–32). Although the cryo-EM structure is not in complex with PIP2, multiple basic residues, including the KRRK cluster, K248 (S4–S5 linker), and R243 (the second arginine in a RR motif conserved in retigabine-sensitive KCNQ channels, at the intracellular end of S4), orient toward a pocket that is a good candidate for a PIP2 binding site that could couple the C-terminal KRRK motif with elements of the voltage sensor and S4–S5 linker (Fig. 8). A PIP2-dependent mechanism of coupling between the C terminus and voltage-sensing apparatus provides a rationale for both poor efficiency of channel opening in KRRK cluster mutants (Fig. S2) or PIP2 reduction (Fig. 3). Moreover, stabilization of this configuration by retigabine would account for the protection of PIP2 against CiVSP-mediated run-down and the loss of protection after neutralization of critical C-terminal or S4–S5 linker residues (Fig. 4). The model highlights our suggestion of PIP2-dependent "bridging" of the C terminus and voltage sensor, which may constrain the voltage sensor, and

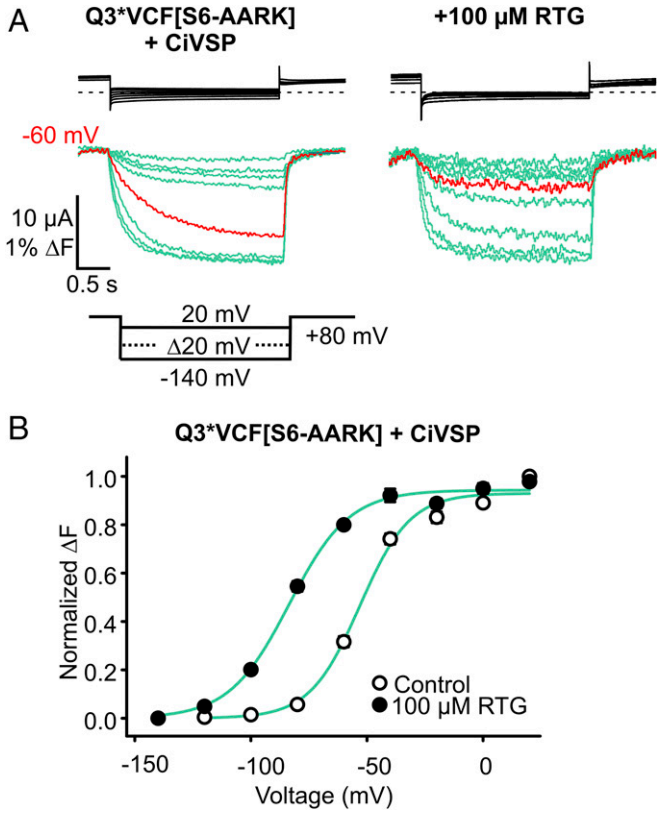

Fig. 7. RTG activates the VSD in "PIP2-less" Q3*VCF [S6-AARK] channels. (*A*) Effects of RTG on the voltage dependence of ΔF from Q3*VCF [S6-AARK] was assessed under PIP2-depleted conditions (by coexpression with CiVSP, using a holding potential of +80 mV for sustained CiVSP activation). Exemplar currents (black) and fluorescence (green) recordings are shown, but no KCNQ currents were detectable. (*B*) Summary of FV relationships in control and 100 μM RTG, highlighting the RTG-induced shift in the absence of PIP2 ($\Delta V_{1/2} = -31 \pm 2$ mV, $n = 4$).

also allow pore binding of retigabine to exert its dramatic effect on voltage sensor deactivation kinetics.

Discussion

Retigabine is a powerful opener of neuronal KCNQ channels, with a well-defined binding site in the channel pore (14, 15, 33). However, mechanisms that couple the pore to the voltage sensing domain, and link retigabine binding to altered voltage sensitivity, are poorly understood. Previous investigations of voltage sensing in KCNQ channels have focused primarily on KCNQ1, demonstrating that VSD movements in KCNQ1 are dynamically regulated by association with auxiliary subunits such as KCNE1/3 and by PIP2, which affect not only the VSD response to voltage, but also coupling of VSD movements to opening of the pore gate (20–22, 34, 35). Although neuronal KCNQ channels like KCNQ3 share this requirement for PIP2, their unique sensitivity to retigabine provides a tool to identify structural motifs that govern the interplay between voltage sensing, pharmacology, and regulation by PIP2.

We found that retigabine shifts the voltage dependence of Q3*VCF fluorescence in parallel with channel conductance, demonstrating drug-mediated stabilization of the activated voltage sensor. At ambient PIP2 levels, KCNQ3 activation was modulated over a wide voltage range with retigabine, and close overlap of the voltage dependence of pore opening and voltage sensor fluorescence was retained (Fig. 2*A*). This close overlap resembles observations made in KCNQ1 in the absence of KCNE1 (21). Disruption of channel:PIP2 interactions caused significant changes of voltage sensor dynamics and pore gating that we describe colloquially as "unhinging" of the voltage sensor from the pore.

An obvious feature of the unhinged voltage sensor was a significantly increased magnitude of the fluorescence signal (Fig. 3 *B–E*). We suggest that this effect reflects the adoption of novel VSD conformations when constraints imposed by PIP2-dependent pore:VSD coupling are removed. The extracellular environment around the fluorescent tag was not manipulated in these experiments, so it seems reasonable to infer that the much larger fluorescence signals after PIP2 reduction (Fig. 3, or disruptive C-terminal mutations such as S6-AARK, Figs. 5–7) indicate a significant change in VSD conformation when uncoupled from the pore. It is noteworthy that KCNQ1 channels (tagged at the

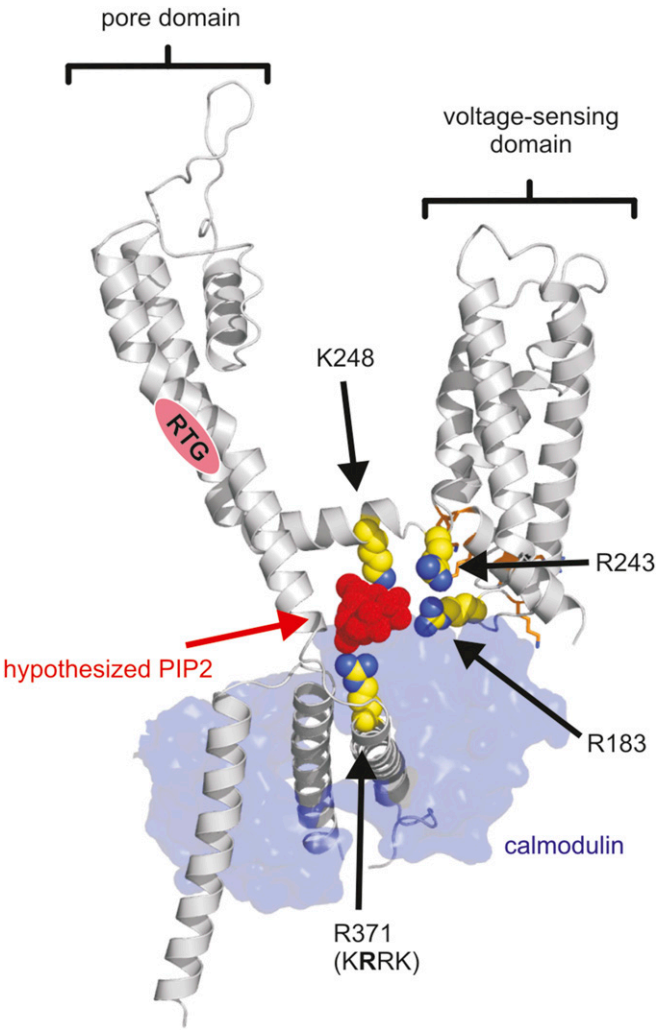

Fig. 8. Proposed PIP2 binding region in a model of KCNQ3. A homology model of KCNQ3 was generated based on a cryo-EM structure of KCNQ1 (PDB 5VMS). Highlighted residues in the proximal C terminus (R371) and S4–S5 linker (K248) were found to have a perturbative effect on current magnitude and retigabine protection against CiVSP-mediated rundown. Other basic amino acid residues delineating a pocket that may accommodate a PIP2 headgroup are highlighted (S4 residue R243). R183 is predicted to be the closest S2–S3 linker residue to this pocket but would be largely occluded by the associated calmodulin subunit (depicted in blue). A hypothesized PIP2 headgroup has been positioned manually in this potential binding pocket to illustrate the approximate dimensions and to highlight our hypothesis.

equivalent position) also exhibit much larger fluorescence changes than we observe in Q3*VCF (20). Although not yet tested directly, one interesting explanation could be the critical KRRX sequence that is present in KCNQ2–5, but not KCNQ1, that may constrain voltage sensor movement relative to KCNQ1 (Figs. 3 and 4). Further evidence for significant impact on voltage sensor function is that the KRRK cluster mutants exhibit steeper fluorescence–voltage relationships compared with Q3*VCF (Fig. 5).

A second feature of the unhinged voltage sensor is altered deactivation kinetics of voltage sensor fluorescence after PIP2 breakdown (Fig. 3*G*) or in KRRK neutralizations such as S6-AARK (Fig. 6). Moreover, deactivation of the unhinged voltage sensor is not strongly decelerated by retigabine, unlike the dramatic effects on Q3*VCF deactivation (Fig. 6). A previous study reported that PIP2 rundown prevents retigabine activation of KCNQ2 channels (36). We were thus surprised to find that despite our best efforts to reduce PIP2 and unhinge the voltage sensor, there was a persistent (although weakened) retigabine-mediated hyperpolarizing shift of the VSD, even in the absence of ionic current (Fig. 7). The shift appears to be due primarily to acceleration of VSD activation kinetics, rather than deceleration of deactivation (Fig. 6), implying that retigabine binding to the pore is communicated in multiple ways to the VSD. Our findings suggest separable PIP2-dependent and PIP2-independent modes of coupling between the KCNQ pore and voltage sensors, which predominantly affect deactivation or activation, respectively (Figs. 6 and 7).

The convergent effects of KRRK mutations and PIP2 depletion in terms of channel function, voltage sensor deactivation, and weakened PIP2 protection, might be rationalized with a structural model as shown (Fig. 8). We suggest that a PIP2-mediated association between the C terminus (adjacent to the S6 gate) and the VSD is essential for normal channel function and sensitivity to retigabine. When PIP2 is abundant, reciprocal interactions between the VSD, PIP2, and pore, may be reflected in closely overlapping fluorescence– and conductance–voltage relationships (Fig. 2). An intuitive explanation is that when the C terminus can closely engage with the voltage sensor (via PIP2), mutual constraints on their motions cause them to operate with similar voltage dependence. However, when PIP2 interactions are disrupted, we suggest that these constraints are weakened or lost, leading to dissociation of FV and GV relationships in certain conditions (Fig. 5 *A* and *B*, notably S6-AARK or S6-AAAA in retigabine). PIP2-independent effects of retigabine on VSD activation (Fig. 6) persist in these mutants, but do not efficiently open channels due to the lack of PIP2 (Fig. 5). Thus, there is likely a large fraction of voltage sensors that generate a fluorescence signal, but do not influence a PIP2-coupled gate. Moreover, the large increase in fluorescence in PIP2-reduced conditions (Fig. 3*B*) suggests that the fluorescence signal from unhinged voltage sensors is larger and this effect may accentuate differences of the FV relative to the GV. Most importantly, even after fairly significant rescue of current by retigabine (see S6-KRAA or S6-AARK in Fig. 5*A*) the open pore and active voltage sensor are not well stabilized by the drug. This is supported by the deactivation of ionic tail currents (Fig. 5*A*) and VSD fluorescence (Fig. 6 *A* and *B*), as both are much faster than Q3*VCF (Fig. 2 *A* and *B*). The influence of retigabine toward stabilizing the engaged C terminus:PIP2:VSD arrangement also emerges in the protection of PIP2 against CiVSP-mediated breakdown (Fig. 4). As mentioned, this mirrors earlier characterizations of retigabine demonstrating protection against M1 receptor-mediated rundown (28). This observation may have important implications related to the therapeutic drug mechanism, suggesting that in addition to silencing neurons through KCNQ channel activation, retigabine may blunt sensitivity to signaling cascades that operate through PLC-mediated PIP2 breakdown.

We did not observe dramatic effects of S2–S3 linker mutations, although certain mutants, such as R190A, exhibited both weaker PIP2 protection and less overall current (Fig. 4 and Fig. S2). These residues may be candidates for future investigation, although the cryo-EM structure suggests that the S2–S3 linker does not directly interact with the KRRK motif or other elements of the C terminus (Fig. 8). In the context of the recent structure, an important issue to unravel will be whether calmodulin plays a role in mediating interactions between the C terminus and VSD. PIP2 and calmodulin may compete in this region, as reported recently for KCNQ1 (37), or interact in some other cooperative manner, with calmodulin contributing to the functional interaction between the C terminus and voltage sensor that we have observed here. Previous work has proposed that the S4–S5 linker also contributes to channel–PIP2 interactions in KCNQ2 and KCNQ3 (18, 36). This is supported by our observation that the S4–S5 linker K248A mutation weakened channel function and retigabine action (Fig. 4*E* and Fig. S2).

Collectively, our findings demonstrate that retigabine actions are strongly influenced by a PIP2-mediated interaction between the pore and VSD, specifically involving a cluster of basic residues in the C terminus of retigabine-sensitive KCNQ channels. The presence of PIP2 is essential for channel opening and affects transduction of retigabine binding to stabilization of the activated conformation of the VSD. Perturbation of this lipid-mediated coupling mechanism causes uncoupling of the pore and VSD in certain conditions and a significant attenuation of retigabine effects. These findings reveal fundamental details of voltage- and lipid-dependent gating in KCNQ channels, together with essential structural determinants underlying retigabine action.

Methods

Molecular Biology. KCNQ3 channel cDNA constructs were expressed using the pSRC5 vector (gifts from M. Taglialatela, University of Molise, Campobasso, Italy, and T. Jentsch, Leibniz-Institut für Molekulare Pharmakologie, Berlin). In all experiments, the Ala315Thr mutation was introduced to enable efficient KCNQ3 functional expression without coinjection of KCNQ2 mRNA {throughout the text we refer to KCNQ3[Ala315Thr] as KCNQ3*}. For VCF recordings, the KCNQ3[A315T][Q218C] mutation was used, and is referred to as Q3*VCF throughout the text. The plasmid encoding CiVSP was kindly provided by Y. Okamura, Osaka University, Osaka. cRNA was transcribed from the cDNA using the mMessage mMachine kit (Ambion). Stage V–VI *Xenopus laevis* oocytes were prepared as previously described and injected with 50 ng of channel cRNA with or without 15 ng CiVSP cRNA. After injection, oocytes were incubated for 24–72 h at 17 °C before recording.

Two-Electrode Voltage Clamp and VCF. Voltage-clamped potassium currents were recorded in modified Ringer's solution (in millimoles): 116 NaCl, 2 KCl, 1 MgCl2, 0.5 CaCl2, 5 Hepes (pH 7.4) using an OC-725C voltage clamp (Warner). Glass microelectrodes were backfilled with 3 M KCl and had resistances of 0.1–1 MΩ. Data were filtered at 5 kHz and digitized at 10 kHz using a Digidata 1440A (Molecular Devices) controlled by pClamp 10 software (Molecular Devices). Retigabine was purchased from Toronto Research Chemicals and stored as 100-mM stocks in DMSO and diluted to working concentrations each experimental day. For VCF, *X. laevis* oocytes expressing Q3*VCF were incubated in 100 μM Alexa Fluor-488 maleimide (Thermo Fisher Scientific) for 20 min in a depolarizing high K^+ modified Ringer's solution (in millimoles): 100 mM KCl, 1 MgCl2, 0.5 CaCl2, 5 Hepes (pH 7.4). Following labeling, oocytes were thoroughly rinsed in standard Ringer's solution and kept on ice for prompt use. Fluorometry was simultaneously performed with a two-electrode voltage clamp on an Olympus IX51 inverted microscope. A PhlatLight LED (Luminus Devices) powered by a DC power supply (F25-12-AG; Bel Power Solutions) served as the light source, and emitting light from the oocyte animal pole was collected and amplified as an electric signal using a PIN040-A photodiode (OSI Optoelectronics) connected to a patch-clamp head unit/amplifier in voltage-clamp mode (Axopatch-1C; Axon instruments).

Data Analysis. Voltage dependence of channel activation and normalized fluorescence change was fitted with a standard single component Boltzmann equation of the form $G/Gmax = 1/(1 + e^{[-(V - V_{1/2})/k]})$, where $V_{1/2}$ is the voltage

where channels exhibit half-maximal activation, and k is a slope factor reflecting the voltage range over which an e-fold change is observed. Fluorescence data were low-pass filtered at 20 Hz and adjusted for bleaching by subtracting a linear component fitted to the baseline fluorescence at the beginning and end of each voltage sweep. To minimize the impact of bleaching, only data from cells displaying a >0.5% maximal ΔF were used for analysis. ΔF values were obtained by dividing the maximal fluorescence change at the end of the test pulse by the baseline fluorescence preceding the test pulse, from single nonaveraged sweeps. Statistical tests and significance are described in figure legends throughout the text.

Construction of Molecular Model. The molecular model of KCNQ3 was generated using a homology model of KCNQ3 based on the recently published cryo-EM structure of KCNQ1 in complex with calmodulin (Protein Data Bank 5VMS) using the online SWISS-MODEL tool (https://swissmodel.expasy.org) (38). An energy-minimized conformation of the PIP(4,5)2 headgroup was manually docked into the KCNQ3 molecular model for illustration of the dimensions of the pocket and visualization of our hypothesis. We emphasize that this is a preliminary structural model intended to illustrate our hypothesis, and that much further development and refinement of the model will be possible as further constraints are collected.

1. Delmas P, Brown DA (2005) Pathways modulating neural KCNQ/M (Kv7) potassium channels. *Nat Rev Neurosci* 6:850–862.
2. Wang H-S, et al. (1998) KCNQ2 and KCNQ3 potassium channel subunits: Molecular correlates of the M-channel. *Science* 282:1890–1893.
3. Charlier C, et al. (1998) A pore mutation in a novel KQT-like potassium channel gene in an idiopathic epilepsy family. *Nat Genet* 18:53–55.
4. Singh NA, et al. (1998) A novel potassium channel gene, KCNQ2, is mutated in an inherited epilepsy of newborns. *Nat Genet* 18:25–29.
5. Devaux JJ, Kleopa KA, Cooper EC, Scherer SS (2004) KCNQ2 is a nodal K+ channel. *J Neurosci* 24:1236–1244.
6. Pan Z, et al. (2006) A common ankyrin-G-based mechanism retains KCNQ and NaV channels at electrically active domains of the axon. *J Neurosci* 26:2599–2613.
7. Brodie MJ, et al.; RESTORE 2 Study Group (2010) Efficacy and safety of adjunctive ezogabine (retigabine) in refractory partial epilepsy. *Neurology* 75:1817–1824.
8. French JA, et al.; RESTORE 1/Study 301 Investigators (2011) Randomized, double-blind, placebo-controlled trial of ezogabine (retigabine) in partial epilepsy. *Neurology* 76:1555–1563.
9. Porter RJ, Partiot A, Sachdeo R, Nohria V, Alves WM; 205 Study Group (2007) Randomized, multicenter, dose-ranging trial of retigabine for partial-onset seizures. *Neurology* 68:1197–1204.
10. Main MJ, et al. (2000) Modulation of KCNQ2/3 potassium channels by the novel anticonvulsant retigabine. *Mol Pharmacol* 58:253–262.
11. Rundfeldt C, Netzer R (2000) The novel anticonvulsant retigabine activates M-currents in Chinese hamster ovary-cells tranfected with human KCNQ2/3 subunits. *Neurosci Lett* 282:73–76.
12. Tatulian L, Brown DA (2003) Effect of the KCNQ potassium channel opener retigabine on single KCNQ2/3 channels expressed in CHO cells. *J Physiol* 549:57–63.
13. Wickenden AD, Yu W, Zou A, Jegla T, Wagoner PK (2000) Retigabine, a novel anticonvulsant, enhances activation of KCNQ2/Q3 potassium channels. *Mol Pharmacol* 58:591–600.
14. Kim RY, et al. (2015) Atomic basis for therapeutic activation of neuronal potassium channels. *Nat Commun* 6:8116.
15. Lange W, et al. (2009) Refinement of the binding site and mode of action of the anticonvulsant Retigabine on KCNQ K+ channels. *Mol Pharmacol* 75:272–280.
16. Schwake M, et al. (2006) Structural determinants of M-type KCNQ (Kv7) K+ channel assembly. *J Neurosci* 26:3757–3766.
17. Wuttke TV, Seebohm G, Bail S, Maljevic S, Lerche H (2005) The new anticonvulsant retigabine favors voltage-dependent opening of the Kv7.2 (KCNQ2) channel by binding to its activation gate. *Mol Pharmacol* 67:1009–1017.
18. Zhou P, et al. (2013) Phosphatidylinositol 4,5-bisphosphate alters pharmacological selectivity for epilepsy-causing KCNQ potassium channels. *Proc Natl Acad Sci USA* 110:8726–8731.
19. Zaika O, Hernandez CC, Bal M, Tolstykh GP, Shapiro MS (2008) Determinants within the turret and pore-loop domains of KCNQ3 K+ channels governing functional activity. *Biophys J* 95:5121–5137.
20. Barro-Soria R, et al. (2014) KCNE1 divides the voltage sensor movement in KCNQ1/KCNE1 channels into two steps. *Nat Commun* 5:3750.
21. Osteen JD, et al. (2010) KCNE1 alters the voltage sensor movements necessary to open the KCNQ1 channel gate. *Proc Natl Acad Sci USA* 107:22710–22715.
22. Zaydman MA, et al. (2013) Kv7.1 ion channels require a lipid to couple voltage sensing to pore opening. *Proc Natl Acad Sci USA* 110:13180–13185.
23. Suh B-C, Inoue T, Meyer T, Hille B (2006) Rapid chemically induced changes of PtdIns(4,5)P2 gate KCNQ ion channels. *Science* 314:1454–1457.
24. Zhang H, et al. (2003) PIP(2) activates KCNQ channels, and its hydrolysis underlies receptor-mediated inhibition of M currents. *Neuron* 37:963–975.
25. Zaydman MA, Cui J (2014) PIP2 regulation of KCNQ channels: Biophysical and molecular mechanisms for lipid modulation of voltage-dependent gating. *Front Physiol* 5:195.
26. Murata Y, Iwasaki H, Sasaki M, Inaba K, Okamura Y (2005) Phosphoinositide phosphatase activity coupled to an intrinsic voltage sensor. *Nature* 435:1239–1243.
27. Murata Y, Okamura Y (2007) Depolarization activates the phosphoinositide phosphatase Ci-VSP, as detected in Xenopus oocytes coexpressing sensors of PIP2. *J Physiol* 583:875–889.
28. Tatulian L, Delmas P, Abogadie FC, Brown DA (2001) Activation of expressed KCNQ potassium currents and native neuronal M-type potassium currents by the anticonvulsant drug retigabine. *J Neurosci* 21:5535–5545.
29. Sun J, MacKinnon R (2017) Cryo-EM structure of a KCNQ1/CaM complex reveals insights into congenital long QT syndrome. *Cell* 169:1042–1050.e9.
30. Wen H, Levitan IB (2002) Calmodulin is an auxiliary subunit of KCNQ2/3 potassium channels. *J Neurosci* 22:7991–8001.
31. Yus-Najera E, Santana-Castro I, Villarroel A (2002) The identification and characterization of a noncontinuous calmodulin-binding site in noninactivating voltage-dependent KCNQ potassium channels. *J Biol Chem* 277:28545–28553.
32. Gamper N, Shapiro MS (2003) Calmodulin mediates Ca2+-dependent modulation of M-type K+ channels. *J Gen Physiol* 122:17–31.
33. Schenzer A, et al. (2005) Molecular determinants of KCNQ (Kv7) K+ channel sensitivity to the anticonvulsant retigabine. *J Neurosci* 25:5051–5060.
34. Barro-Soria R, Perez ME, Larsson HP (2015) KCNE3 acts by promoting voltage sensor activation in KCNQ1. *Proc Natl Acad Sci USA* 112:E7286–E7292.
35. Ruscic KJ, et al. (2013) IKs channels open slowly because KCNE1 accessory subunits slow the movement of S4 voltage sensors in KCNQ1 pore-forming subunits. *Proc Natl Acad Sci USA* 110:E559–E566.
36. Zhang Q, et al. (2013) Dynamic PIP2 interactions with voltage sensor elements contribute to KCNQ2 channel gating. *Proc Natl Acad Sci USA* 110:20093–20098.
37. Tobelaim WS, et al. (2017) Competition of calcified calmodulin N lobe and PIP2 to an LQT mutation site in Kv7.1 channel. *Proc Natl Acad Sci USA* 114:E869–E878.
38. Kiefer F, Arnold K, Kunzli M, Bordoli L, Schwede T (2009) The SWISS-MODEL repository and associated resources. *Nucleic Acids Res* 37:D387–D392.